Decarbonylation and decarboxylation of propanoic acid on Pd_{55} clusters: a quantum chemical modeling

R. S. Shamsiev

MIREA — Russian Technological University, M. V. Lomonosov Institute of Fine Chemical Technologies, 86 prosp. Vernadskogo, 119571 Moscow, Russian Federation.
E-mail: shamsiev.r@gmail.com

The reaction mechanisms of the decarbonylation and decarboxylation of propanoic acid on icosahedral and cuboctahedral clusters Pd_{55} were modeled in terms of the density functional theory using the PBE functional and the SBK pseudopotential. According to calculations, the hydrogen abstraction step of the decarboxylation reaction is the most sensitive to the cluster shape and proceeds more readily on the icosahedral cluster. The activation energy difference reaches a value of 4.4 kcal mol^{-1}. In addition, the icosahedral cluster demonstrates a higher activity and selectivity toward decarboxylation compared to the cuboctahedral cluster.

Key words: palladium nanoparticles, clusters, decarbonylation, decarboxylation, propanoic acid, density functional theory.

Recently, catalytic chemistry based on the use of renewable raw materials has been intensively developing field of basic and industrial researches.[1—4] Among the most important areas of investigation, there are the development of technologies for production of biofuel by hydrolysis of triglycerides and subsequent deoxygenation of fatty acids to hydrocarbons, as well as the design of highly efficient catalysts. A key step in production of hydrocarbons from acids[5—7] is the removal of oxygen by hydrodeoxygenation or deoxygenation. In the former case the process proceeds with retention of the number of C atoms, while in the latter case oxygen is removed in the form of CO_2 (decarboxylation) or CO and H_2O (decarbonylation). Unlike hydrodeoxygenation, the deoxygenation of fatty acids requires consumption of a much smaller amount of H_2. Fats are suitable to obtain not only higher hydrocarbons, but also higher olefins,[8] *i.e.*, semiproducts that are utilized as a feedstock for production of detergents, synthetic oils, additives, *etc*.

The use of Pd-based catalysts supported on various materials in the deoxygenation reactions of higher fatty acids is of considerable interest.[1,2,6,7,9—11] The main deoxygenation pathways of fatty acids on Pd catalysts are the decarboxylation and decarbonylation reactions. The kinetics and mechanism of these processes in the presence of various metals have been studied.[11—17] A theoretical study[13] of the reaction mechanism of the decarboxylation of propanoic acid on the Pd(111) surface showed that it involves adsorption of propanoic acid, successive abstraction of H atoms from the carboxyl group and from the C_β atom, dissociation of the C—C bond with elimination of CO_2 molecule, and hydrogenation of ethylene to ethane. However, from the periodic density functional theory (DFT) calculations it follows that dissociation of the C—C bond is preceded by deeper dehydrogenation of the C_α atom in propanoic[14,15] and acetic[16] acids to MeCCOO and CHCOO, respectively.

It was reported[13] that the mechanism of propionic acid decarbonylation on the Pd_{13} and Pd_{30} clusters represents the following sequence of steps: $EtCOOH \rightarrow EtCO \rightarrow Et \rightarrow C_2H_4$. Prior to dissociation of the C—C bond the EtCO species on the Pd(100) and Pd(111) surface can undergo dehydrogenation[14,18] to MeCCO, CH_2CHCO, or CHCHCO. In spite of different nature of the rate-limiting steps of the decarbonylation and decarboxylation reactions (dehydrogenation of the C_β atom or dissociation of the C—C and C—OH bonds), the activation barriers to these processes are close, which provides an explanation for the experimentally observed composition of reaction products characteristic of both pathways.

The catalytic activity of nanoparticles depends not only on their size, but also on the surface morphology.[19] Of particular interest for catalysis are metal nanoparticles 2—10 nm in size containing a high fraction of surface atoms that mainly form the low-index

Published in Russian in *Izvestiya Akademii Nauk. Seriya Khimicheskaya,* No. 9, pp. 1863—1869, September, 2022.

faces (111) and (100). The shape of Pd nanoparticles significantly influences the kinetics of selective hydrogenation of hydrocarbons,[20,21] CO oxidation,[22] cross-coupling reactions,[23] *etc*. Recently developed methods for the synthesis of various shape-controlled metal nanoparticles[24–26] offered prospects for the preparation of highly active and selective catalysts. In turn, theoretical prediction of the catalytic properties of particularly shaped particles enables targeted synthesis of novel catalysts. The aim of this work was to model the reaction mechanisms of the decarboxylation and decarbonylation of propanoic acid on icosahedral and cuboctahedral Pd_{55} nanoclusters in order to assess the relative catalytic activities of these nanoparticles.

Calculation Procedure

Quantum chemical calculations were carried out using the PRIRODA program[27,28] in terms of the DFT with the PBE exchange-correlation functional,[29] the SBK relativistic effective core potential,[30] and the TZ2P basis set. The atomic charges were evaluated according to Hirshfeld.[31]

The active site models included two 55-atom Pd clusters, namely, an icosahedral cluster (Pd_{55}^{i}) and a cuboctahedral one (Pd_{55}^{c}). They were chosen because the surface of the Pd_{55}^{i} cluster is composed of the (111) faces only, while the surface of the Pd_{55}^{c} cluster is composed of the (111) and (100) faces. There are two types of equivalent surface atoms in the Pd_{55}^{i} cluster, *viz.*, the vertex atoms (Pd_t) and the edge atoms (Pd_e) with a coordination number (CN) of 6 and 8, respectively. The vertex atoms (Pd_t) and the edge atoms (Pd_e) in the cuboctahedral cluster Pd_{55}^{c} have lower CN equal to 5 and 7, respectively. An additional, third type of surface Pd atoms, appears in the Pd_{55}^{c} cluster. These are the atoms located at the centers of the (100) Pd faces. They have a CN 8 and will be denoted by Pd_s.

According to our calculations, the triplet state lies 10.00 (Pd_{55}^{i}) and 1.93 kcal mol^{-1} (Pd_{55}^{c}) lower than the singlet state on the energy scale and 1.40 (Pd_{55}^{i}) and 0.20 kcal mol^{-1} (Pd_{55}^{c}) than the quintet state. In this connection all other calculations were carried out for the triplet state.

The relative stabilities of the clusters were assessed from the atomization energies (E_b) calculated per atom:

$$E_b = (55 \cdot E(Pd) - E(Pd_{55}))/55.$$

Geometry optimization of all structures was carried out without imposing symmetry restrictions.

The coordinates of the Pd atoms were not fixed in the calculations. The correspondence between the optimized structures and the energy minima or transition states (TS) was confirmed by vibrational frequency analysis.

Results and Discussion

Table 1 presents selected structural and electronic parameters of the clusters Pd_{55}^{i} and Pd_{55}^{c}. The atomization energy (E_b) of the icosahedral cluster is 0.34 kcal mol^{-1} higher than $E_b(Pd_{55}^{c})$, which suggests that Pd_{55}^{i} is more thermodynamically stable. The estimates obtained in this work (E_b = 64.49 and 64.15 kcal mol^{-1}) are in good agreement with the results of a DFT-BP86 study[32] (E_b = 63.32 and 63.30 kcal mol^{-1}, respectively).

Table 1. Atomization energies (E_b) in the Pd_{55}^{i} and Pd_{55}^{c} clusters, Pd—Pd bond lengths in the cluster shell, charges of Pd atoms (δ), and the net charges of the (Pd_{42}) shell

Cluster	E_b /kcal mol^{-1} atom^{-1}	R(Pd—Pd) /Å	δ/au			
			Pd_t	Pd_e	Pd_s	Pd_{42}
Pd_{55}^{i}	64.49	2.78—2.86	0.01	–0.02	—	–0.39
Pd_{55}^{c}	64.15	2.69—2.82	0.01	–0.02	–0.01	–0.30

The bond lengths in the shell of the Pd_{55}^{i} cluster are on the average 0.05 Å longer than in the shell of the Pd_{55}^{c} cluster. The shortest bond lengths R(Pd—Pd) correspond to the Pd_t—Pd_e (Pd_{55}^{i}) and Pd_s—Pd_e (Pd_{55}^{c}) distances, while the longest ones correspond to the Pd_e—Pd_e distances. The outer size of both clusters differ only slightly, namely, 10.6 (Pd_{55}^{i}) *vs.* 10.9 Å (Pd_{55}^{c}).

The edge atoms Pd_e of both clusters bear a small negative charge δ(Pd) = –0.02 au, while the vertex atoms Pd_t bear a small positive charge of 0.01 au (see Table 1). The net charge of the surface atoms in the Pd_{55}^{i} cluster (–0.39 au) is larger than in the Pd_{55}^{c} cluster (–0.30 au).

The strongest adsorption complex is formed when the propanoic acid molecule and the COOH group directed toward the Pd surface are arranged perpendicularly to each other. The major contribution to the adsorption energy comes from the interaction between the carboxyl O atom and the Pd atom (Fig. 1). Table 2 lists the adsorption energies (E_{ads}) of EtCOOH for different types of surface Pd atoms bonded to the O atom. It follows that adsorption on the low-coordinate Pd_t atoms is characterized by the highest energy and E_{ads}(EtCOOH) for the Pd_{55}^{i} cluster (**AC^{i}**, see Fig. 1) is 1.8 kcal mol^{-1} higher in absolute value than for the Pd_{55}^{c} cluster (**AC^{c}**, see Fig. 1). The lowest activity was found for the central atoms Pd_s of the (100) face. Probably, the Pd_s atoms will also exhibit the lowest activity in the dissociation of the C—C and C—OH bonds, because these key steps require high coordinative accessibility of the surface atoms.[33] The mechanism of the decarboxylation and decarbonylation reactions was based on the sequence of steps obtained[13] in the calculations using a small cluster Pd_{13}.

Mechanisms of propanoic acid decarboxylation and decarbonylation on Pd_{55}^{i}. The optimized structures of the intermediates of propanoic acid decarboxylation

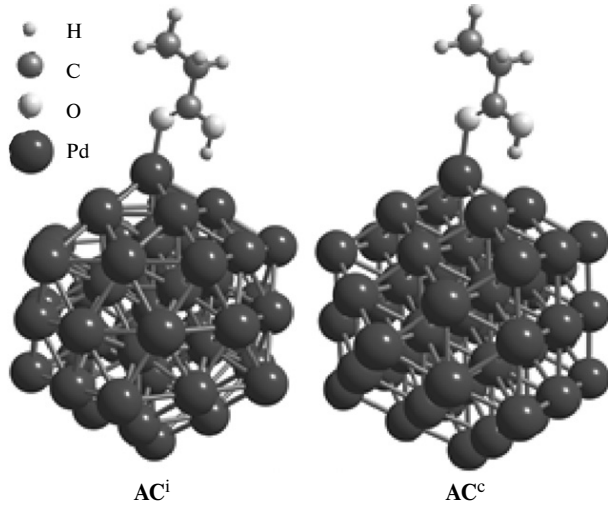

Fig. 1. Optimized structures of adsorption complexes of propanoic acid with icosahedral (**AC^i**) and cuboctahedral (**AC^c**) clusters Pd_{55}.

Table 2. Pd—O bond length in the clusters $Pd_{55}{}^i$ and $Pd_{55}{}^c$ and the adsorption energies of EtCOOH on these clusters

Cluster	Atom	R(Pd—O)/Å	$-\Delta E_{ads}$/ kcal mol^{-1}
$Pd_{55}{}^i$	Pd_t	2.15	20.0
	Pd_e	2.19	16.1
$Pd_{55}{}^c$	Pd_t	2.18	18.2
	Pd_e	2.21	14.4
	Pd_s	2.25	9.8

(**I1a^i**—**I5a^i**) and decarbonylation (**I1b^i**—**I5b^i**) on the icosahedral cluster $Pd_{55}{}^i$ are shown in Fig. 2. Hydrogen abstraction from the carboxyl group in the first step of decarboxylation on the surface of the $Pd_{55}{}^i$ cluster produces the EtCOO* species (**I1a^i**) that is 4 kcal mol^{-1} more stable than **AC^i** owing to the interaction between two O atoms (μ_2-coordination) with Pd atoms.

The key step of the decarboxylation mechanism involves dissociation of the C—C bond which should be preceded[8] by abstraction of the H atom from the C_β atom of EtCOO* to decrease the activation barrier to dissociation of the C—C bond.[14] Dehydrogenation results in the intermediate **I2a^i** with the shortest distance between the CH_2CH_2COO* species and the surface of the Pd cluster, which creates structural prerequisites for further transformations.

Dissociation of the C—C bond is accompanied by noticeable exothermic effect (ΔE(**I2a^i**→**I3a^i**) = = −12.7 kcal mol^{-1}) and results in the formation of adsorbed ethylene and CO_2 molecules (**I3a^i**). Two adsorbed H atoms formed in the preceding steps are consumed for successive hydrogenation of ethylene to ethyl (**I4a^i**) and ethane (**I5a^i**).

The energy profiles of the reactions of propanoic acid decarboxylation and decarbonylation on the $Pd_{55}{}^i$ cluster are shown in Fig. 3. As can be seen, the activation energy of decarboxylation (30.7 kcal mol^{-1}) is determined by the energy difference between the intermediate **I1a^i** (lowest point of the energy profile) and the TS of the step **I2a^i**→**I3a^i** (highest point of the energy profile).

In the first step of the decarbonylation reaction the COOH group of the adsorbed propanoic acid molecule (**AC^i**, see Fig. 1) approaches the surface of the $Pd_{55}{}^i$ cluster. As a result, the intermediate **I1b^i** (see Fig. 2) is formed. Its carboxyl C and O atoms interact with three

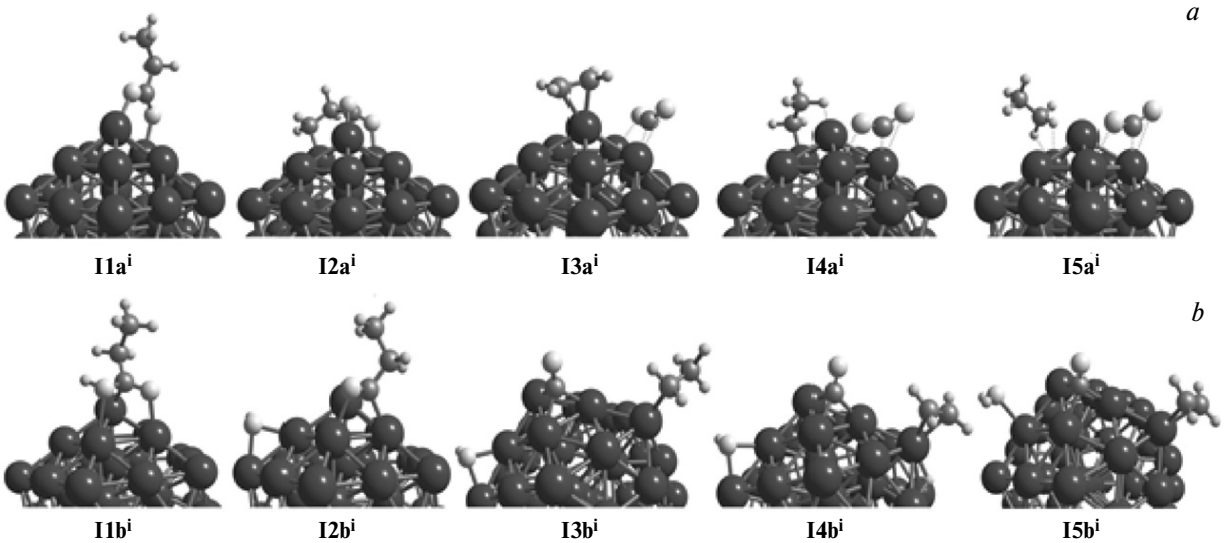

Fig. 2. Optimized structures of intermediates of the reactions of propanoic acid decarboxylation (*a*) and decarbonylation (*b*) on the $Pd_{55}{}^i$ cluster.

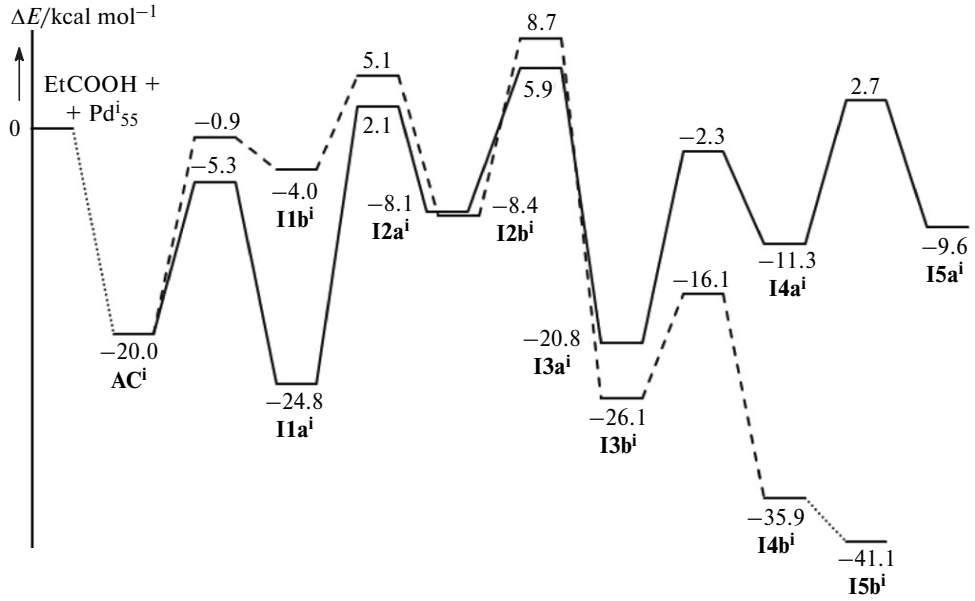

Fig. 3. Energy profiles of propanoic acid decarboxylation (solid line) and decarbonylation (dashed line) on icosahedral cluster Pd_{55}^{i}.

Pd atoms. The formation of the intermediate **I1b^{i}** is energetically unfavorable because the energy increases by 16.0 kcal mol^{-1} relative to **AC^{i}**; however, the OH group can be eliminated with a low activation barrier ($\Delta E^{\neq}$(**I1b^{i}**→**I2b^{i}**) = 9.1 kcal mol^{-1}) only in this case. The second step involving elimination of the OH group leads to the species EtCO* and OH* (**I2b^{i}**, see Fig. 2).

Dissociation of the C—C bond is characterized by a high exothermic effect (ΔE(**I2b^{i}**→**I3b^{i}**) = = −17.7 kcal mol^{-1}), being followed by the formation of two adsorbed molecules, Et* and CO* (**I3b^{i}**). In accordance with the stoichiometry of the decarbonylation reaction Et* undergoes further dehydrogenation to ethylene (**I4b^{i}**). The final step involves the formation of water molecule (**I5b^{i}**, see Fig. 2) with a low energy barrier. Surface migration of H atoms over the Pd_{55} cluster was not considered because of the low activation barriers to this process (<2 kcal mol^{-1}).[34]

The energy profile of the decarbonylation reaction (Fig. 3) demonstrates that the highest energy corresponds to dissociation of the C—C bond (**I2b^{i}**→**I3b^{i}**) rather than elimination of the OH group (**I1b^{i}**→**I2b^{i}**), as was found for the small cluster Pd_{13}.[13] Therefore, the activation energy of this reaction (28.7 kcal mol^{-1}) will be determined by the energy difference between the TS of C—C bond dissociation and the adsorption complex **AC^{i}**. On the other hand, taking into account the equilibrium **AC^{i}**→**I1a^{i}**, it is more correctly to calculate the activation energy with respect to **I1a^{i}**, which gives a value of 33.5 kcal mol^{-1}.

Mechanisms of propanoic acid decarboxylation and decarbonylation on Pd_{55}^{c}. Figure 4 presents the optimized structures of the intermediates of propanoic acid decarboxylation (**I1a^{c}**—**I5a^{c}**) and decarbonylation (**I1b^{c}**—**I5b^{c}**) on the cuboctahedral cluster Pd_{55}^{c} while Fig. 5 shows the corresponding energy profiles. The reaction mechanisms were modeled using the same sequence of steps as that considered for the icosahedral cluster Pd_{55}^{i}.

A comparison of the energy profiles of the reactions on the Pd_{55}^{i} (see Fig. 3) and Pd_{55}^{c} (see Fig. 5) clusters revealed only insignificant differences. This first of all concerns the relative energies of intermediates. For instance, the intermediates **I1a^{c}** and **I5a^{c}** of the decarboxylation reaction are respectively 0.3 and 4.6 kcal mol^{-1} more stable than their analogues **I1a^{i}** and **I5a^{i}**, while the intermediates **I2a^{c}**, **I3a^{c}**, and **I4a^{c}** are 1.3—2.5 kcal mol^{-1} less stable than the corresponding intermediates **I2a^{i}**, **I3a^{i}**, and **I4a^{i}**. The opposite trend was noted for the decarbonylation reaction, *viz.*, all intermediates of the reaction on the cluster Pd_{55}^{c}, except **I5b^{c}**, are 0.3—2.3 kcal mol^{-1} energetically more favorable than their analogues formed in the reaction on the cluster Pd_{55}^{i}.

The next difference is related to the close values of the energies of the highest-lying TS. For instance, the energy difference between the TS of hydrogen abstraction (**I1a^{c}**→**I2a^{c}**) and the TS of C—C bond dissociation (**I2a^{c}**→**I3a^{c}**) is 0.2 kcal mol^{-1} *vs* 0.9 kcal mol^{-1} for the energy difference between the TS of dissociation of the C—OH (**I1b^{c}**→**I2b^{c}**) and C—C (**I2b^{c}**→**I3b^{c}**) bonds. The TS energies for these steps on the cluster Pd_{55}^{c} are almost the same, being noticeably different (by 2.6—4.7 kcal mol^{-1}) for the reaction on the Pd_{55}^{i} cluster.

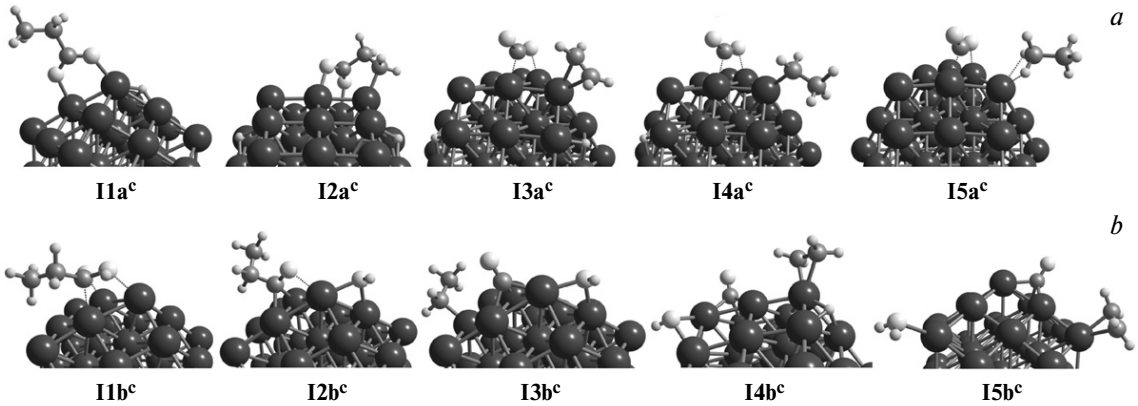

Fig. 4. Optimized structures of intermediates of the reactions of propanoic acid decarboxylation (*a*) and decarbonylation (*b*) on the $Pd_{55}{}^{c}$ cluster.

Table 3 lists the TS energies of the dissociation of the C—H ($E^{\neq}_{C-H}$(**I1a^{i}→I2a^{i}**), $E^{\neq}_{C-H}$(**I1a^{c}→I2a^{c}**)) and C—C ($E^{\neq}_{C-C}$(**I2a^{i}→I3a^{i}**), $E^{\neq}_{C-C}$(**I2a^{c}→I3a^{c}**)) bonds in the decarboxylation reaction, as well as the TS energies of the dissociation of the C—OH ($E^{\neq}_{C-OH}$(**I1b^{i}→I2b^{i}**), $E^{\neq}_{C-OH}$(**I1b^{c}→I2b^{c}**)) and C—C ($E^{\neq}_{C-C}$(**I2b^{i}→I3b^{i}**), $E^{\neq}_{C-C}$(**I2b^{c}→I3b^{c}**)) bonds in the decarbonylation reaction. It follows that hydrogen abstraction in the course of the decarboxylation reaction is the most sensitive to the structure of the Pd cluster. The energy barrier to this step (**I1a^{i}→I2a^{i}**) for the reaction on the icosahedral cluster is 4.4 kcal mol^{-1} lower compared to the process on the cuboctahedral cluster. Besides, dissociation of the C—C bond in the course of the decarboxylation reaction on the $Pd_{55}{}^{i}$ cluster also proceeds more readily; however, in this case the energy difference between the reactions on $Pd_{55}{}^{i}$ and $Pd_{55}{}^{c}$ is small (0.8 kcal mol^{-1}).

Table 3. Transition-state energies (kcal mol^{-1}) for selected steps of the reactions of propanoic acid decarboxylation (DCX) and decarbonylation (DCN) on the $Pd_{55}{}^{i}$ and $Pd_{55}{}^{c}$ clusters calculated relative to the energies of **I1a^{i}** and **I1a^{c}** for the reactions on $Pd_{55}{}^{i}$ and $Pd_{55}{}^{c}$, respectively

Cluster	DCX		DCN	
	$E^{\neq}_{C-H}$ (**I1a→I2a**)	$E^{\neq}_{C-C}$ (**I2a→I3a**)	$E^{\neq}_{C-OH}$ (**I1b→I2b**)	$E^{\neq}_{C-C}$ (**I2b→I3b**)
$Pd_{55}{}^{i}$	26.9	30.7	29.9	33.5
$Pd_{55}{}^{c}$	31.3	31.5	30.8	31.7

Both reactions on the $Pd_{55}{}^{c}$ cluster proceed with close activation energies (31.7 and 31.5 kcal mol^{-1}). It

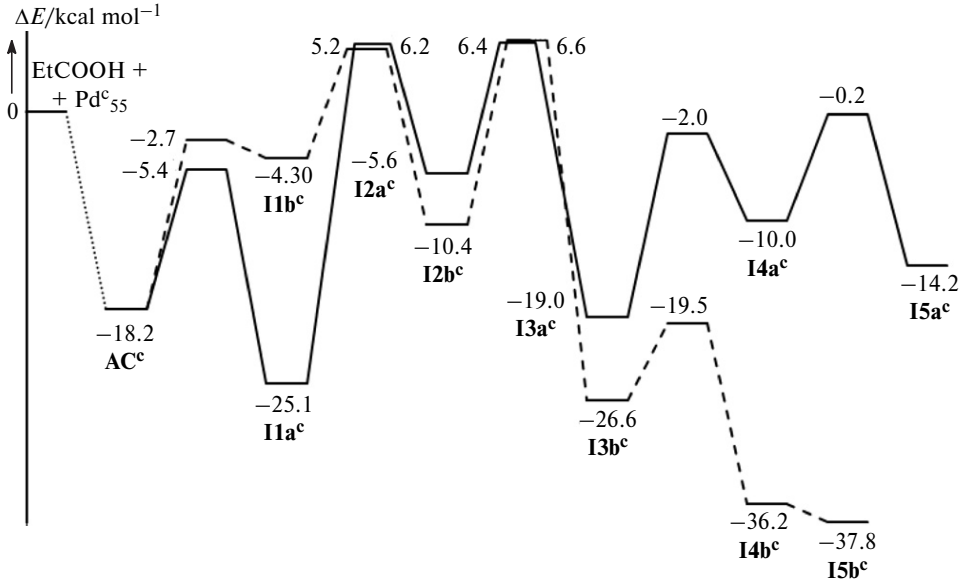

Fig. 5. Energy profiles of propanoic acid decarboxylation (solid line) and decarbonylation (dashed line) on cuboctahedral cluster $Pd_{55}{}^{c}$.

follows that the selectivity of the process on the cuboctahedral cluster is low. A comparison of the energies $E^{\neq}_{C-C}$(DCX) and $E^{\neq}_{C-C}$(DCN) suggests that the $Pd_{55}{}^{i}$ cluster demonstrates a higher activity (compared to $Pd_{55}{}^{c}$) and selectivity toward decarboxylation. This result is more probably due to steric rather than electronic effects because of the close values of the charges on the shell atoms in both clusters (see Table 1). For instance, dissociation of the C—C bond in the species $*C_2H_4CO_2$ (**I2a**) proceeds on one Pd atom *vs*. two Pd atoms in the case EtCO* (**I2b**).

Summing up, the relative catalytic activities of icosahedral and cuboctahedral clusters Pd_{55} were assessed using the DFT-PBE/SBK quantum chemical modeling of the reaction mechanisms of the decarboxylation and decarbonylation of propanoic acid on the surface of these Pd nanoparticles. According to calculations, in all cases the rate-limiting states correspond to the transition states of C—C bond dissociation and to the intermediate EtCOO*. Hydrogen abstraction in the course of the decarboxylation reaction is the most sensitive to the structure of the Pd cluster. This step proceeds more readily on the icosahedral cluster, the activation energy difference being as high as 4.4 kcal mol^{-1}. In addition, the icosahedral cluster is characterized by higher activity and selectivity toward decarboxylation compared to the cuboctahedral cluster Pd_{55}.

Calculations were carried out on computational facilities at the Joint Supercomputer Center of the Russian Academy of Sciences.

No human or animal subjects were used in this research.

The authors declare no competing interests.

References

1. M. Snåre, I. Kubicková, P. Mäki-Arvela, K. Eränen, D. Yu. Murzin, *Ind. Eng. Chem. Res.*, 2006, **45**, 5708; DOI: 10.1021/ie060334i.
2. A. S. Berenblyum, T. A. Podoplelova, R. S. Shamsiev, E. A. Katsman, V. Ya. Danyushevsky, V. R. Flid, *Catalysis in Industry*, 2012, **4**, 209; DOI: 10.1134/S2070050412030026.
3. G. C. R. Silva, D. Qian, R. Pace, O. Heintz, G. Caboche, E. Santillan-Jimenez, M. Crocker, *Catalysts*, 2020, **10**, 91; DOI: 10.3390/catal10010091.
4. J. Gopeesingh, R. Zhu, R. Schuarca, W. Yang, A. Heyden, J. Q. Bond, *Ind. Eng. Chem. Res.*, 2021, **60**, 16171; DOI: 10.1021/acs.iecr.1c03032.
5. K. A. Rogers, Y. Zheng, *ChemSusChem*, 2016, **9**, 1750; DOI: 10.1002/cssc.201600144.
6. E. Santillan-Jimenez, M. Crocker, *J. Chem. Technol. Biotechnol.*, 2012, **87**, 1041; DOI: 10.1002/jctb.3775.
7. A. S. Berenblyum, V. Ya. Danyushevsky, P. S. Kuznetsov, E. A. Katsman, R. S. Shamsiev, *Petroleum Chemistry* (*Engl. Transl.*), 2016, **56**, 663; DOI: 10.1134/S0965544116080028.
8. E. A. Katsman, V. Ya. Danyushevsky, P. S. Kuznetsov, R. S. Shamsiev, A. S. Berenblyum, *Kinet. Catal.* (*Engl. Transl.*), 2017, **58**, 147; DOI: 10.1134/S0023158417020069.
9. J. P. Ford, J. G. Immer, H. H. Lamb, *Top. Catal.*, 2012, **55**, 175; DOI: 10.1007/s11244-012-9786-2.
10. K. Hengst, M. Arend, R. Pfìtzenreuter, W. F. Hoelderich, *Appl. Catal. B*, 2015, **174—175**, 383; DOI: 10.1016/j.apcatb.2015.03.009.
11. A. S. Berenblyum, T. A. Podoplelova, E. A. Katsman, R. S. Shamsiev, V. Ya. Danyushevsky, *Kinet. Catal.* (*Engl. Transl.*), 2012, **53**, 595; DOI: 10.1134/S0023158412050023.
12. J. Fu, D. Mei, *Catal. Today*, 2021, **365**, 181; DOI: 10.1016/j.cattod.2020.05.014.
13. R. S. Shamsiev, I. E. Sokolov, F. O. Danilov, V. R. Flid, *Kinet. Catal.* (*Engl. Transl.*), 2019, **60**, 627; DOI: 10.1134/S0023158419050094.
14. J. Lu, S. Behtash, A. Heyden, *J. Phys. Chem. C*, 2012, **116**, 14328; DOI: 10.1021/jp301926t.
15. J. Lu, S. Behtash, M. Faheem, A. Heyden, *J. Catal.*, 2013, **305**, 56; DOI: 10.1016/j.jcat.2013.04.026.
16. K. C. Chukwu, L. Árnadóttir, *J. Phys. Chem. C*, 2020, **124**, 13082; DOI: 10.1021/acs.jpcc.0c00436.
17. R. S. Shamsiev, F. O. Danilov, V. R. Flid, *Russ. Chem. Bull.*, 2022, **71**, 220; DOI: 10.1007/s11172-022-3400-y.
18. S. K. Kundu, R. V. Solomon, W. Yang, E. Walker, O. Mamun, J. Q. Bond, A. Heyden, *Catal. Sci. Technol.*, 2021, **11**, 6163; DOI: 10.1039/D1CY01029H.
19. D. Uzio, G. Berhault, *Catal. Rev. Sci. Eng.*, 2010, **52**, 106; DOI: 10.1080/01614940903510496.
20. G. A. Somorjai, J. Y. Park, *Angew. Chem. Int. Ed.*, 2008, **47**, 9212; DOI: 10.1002/anie.200803181.
21. Y. Zhao, G. Fu, N. Zheng, *Catal. Today*, 2017, **279**, 36; DOI: 10.1016/j.cattod.2016.05.017.
22. S. Sreedhala, V. Sudheeshkumar, C. P. Vinod, *J. Catal.*, 2016, **337**, 138; DOI: 10.1016/j.jcat.2016.01.017.
23. G. Collins, M. Schmidt, C. O´Dwyer, J. D. Holmes, G. P. McGlacken, *Angew. Chem., Int. Ed.*, 2014, **53**, 4142; DOI: 10.1002/anie.201400483.
24. A. Ruditskiy, S.-I. Choi, H.-C. Peng, Y. Xia, *MRS Bull.*, 2014, **39**, 727; DOI: 10.1557/mrs.2014.167.
25. Y. Wang, S. Xie, J. Liu, J. Park, C. Z. Huang, Y. Xia, *Nano Lett.*, 2013, **13**, 2276; DOI: 10.1021/nl400893p.
26. N. S. Kuzmina, S. V. Portnova, E. L. Krasnykh, *Fine Chem. Technol.*, 2020, **15**, No. 2, 47; DOI: 10.32362/2410-6593-2020-15-2-47-55.
27. D. N. Laikov, *Chem. Phys. Lett.*, 1997, **281**, 151; DOI: 10.1016/S0009-2614(97)01206-2.
28. D. N. Laikov, Yu. A. Ustynyuk, *Russ. Chem. Bull.*, 2005, **54**, 820; DOI: 10.1007/s11172-005-0329-x.

29. J. P. Perdew, K. Burke, M. Ernzerhof, *Phys. Rev. Lett.*, 1996, **77**, 3865; DOI: 10.1103/PhysRevLett.77.3865.
30. W. J. Stevens, H. Basch, M. Krauss, *J. Chem. Phys.*, 1984, **81**, 6026; DOI: 10.1063/1.447604.
31. F. L. Hirschfeld, *Theoret. Chim. Acta*, 1977, **44**, 129; DOI: 10.1007/BF00549096.
32. P. Nava, M. Sierka, R. Ahlrichs, *Phys. Chem. Chem. Phys.*, 2003, **5**, 3372; DOI: 10.1039/B303347C.
33. R. S. Shamsiev, I. E. Sokolov, V. R. Flid, *Russ. Chem. Bull.*, 2014, **63**, 2585; DOI: 10.1007/s11172-014-0783-4.
34. R. S. Shamsiev, F. O. Danilov, *Russ. Chem. Bull.*, 2017, **66**, 395; DOI: 10.1007/s11172-017-1746-3.

Received March 28, 2022;
in revised form May 11, 2022;
accepted May 12, 2022